Inorganic Chemistry

Article

pubs.acs.org/IC

New Perspective in Garnet Phosphor: Low Temperature Synthesis, Nanostructures, and Observation of Multimodal Luminescence

Kavita Mishra,[†] Sunil Kumar Singh,[*,‡] Akhilesh Kumar Singh,[†,#] Monika Rai,[†] Bipin Kumar Gupta,[§] and Shyam Bahadur Rai[†]

[†]Department of Physics, Banaras Hindu University, Varanasi-221005, India

[‡]Department of Physics, Indian Institute of Technology (Banaras Hindu University), Varanasi-221005, India

[§]National Physical Laboratory (CSIR), Dr K S Krishnan Road, New Delhi-110012, India

Supporting Information

ABSTRACT: Herein, we report a new concept for garnet materials in terms of the synthesis of nanocrystalline structure at low temperatures and its multimodal luminescence processes. Terbium- and ytterbium-ion-codoped yttrium gallium garnet nanophosphors have been synthesized via solution combustion technique; nearly pure phase nanophosphor samples were obtained. The synthesized nanophosphor shows efficient multimodal upconversion (UC), downshifting (DS), and quantum cutting (QC)/downconversion (DC) luminescence, which is a new paradigm in garnet material. The garnet nanophosphor shows strong green emission through DS and UC processes both. Furthermore, cooperative energy transfer (CET) has been described in detail, and a possible mechanism for the QC process is also proposed. A UV/blue photon absorbed by Tb^{3+} ion splits into two near-infrared photons (wavelength range 900−1040 nm), emitted by a Yb^{3+} ion pair, with an efficiency of more than 100%. The Yb^{3+} concentration dependent ET from Tb^{3+} to Yb^{3+} has been verified using time domain analysis. An ET efficiency as high as 28% and a corresponding QC efficiency of about 128% (for 15 mol % of Yb^{3+} concentration) have been attained. Such a multimode emitting nanophosphor could be very useful in display devices and for enhancing the conversion efficiency of next generation solar cells via spectral modification etc.

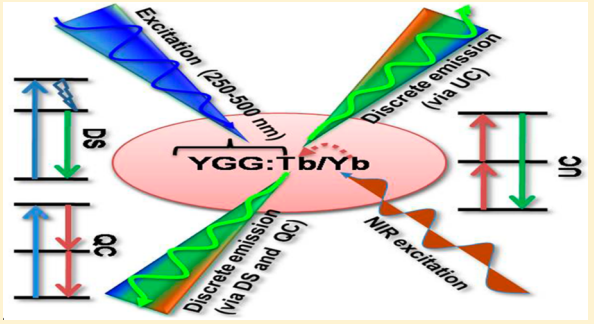

1. INTRODUCTION

High thermal stability, hardness, optical isotropy, good thermal conductivity, etc. make garnets a useful host for various optical applications, particularly for lasing and solid state lighting applications.[1−7] Garnets are basically a combination of Ln_2O_3 (rare earth oxide) and M_2O_3 (metal oxide), where Ln = Y, Gd and M = Al, Ga. Garnets can be described by the $\{A\}_3[B]_2(C)_3O_{12}$ formula, where A (Y^{3+}) is a dodecahedrally coordinated site with point group D_2 (without inversion center), while B (Al^{3+}) and C (Al^{3+}) are octahedrally and tetrahedrally coordinated sites with C_{3i} (with inversion center) and S_4 point groups, respectively.[5] Because of similar ionic radii and chemical properties, Y^{3+}/Gd^{3+} ions can easily be replaced by other lanthanide ions (e.g., Eu^{3+}, Nd^{3+}, Tm^{3+}, Er^{3+}, Tb^{3+}) in the crystal lattice, making garnets optically active material.[6,7]

The synthesis of garnets is usually accomplished through a conventional solid state reaction method at a high temperature (above 1300 °C) which causes heterogeneity in the material.[7−9] Furthermore, such a high temperature synthesis causes coarsening of the grains and leads to the development of micron sized particles, which pertains to constraints in utilizing the garnet material for modern optical applications, particularly triggered due to advancement in nanotechnology, such as in biophotonics, energy harvesting, etc.[10,11] In this context, the solution combustion method is a simple, economically viable, and convenient synthesis technique and shows advantages of synthesis at low temperature, homogeneous composition throughout, fine grains on the order of nano sized etc. when compared to the solid state reaction method. In fact, the synthesis of a few hosts from the garnet family such as yttrium aluminum garnet (YAG), yttrium iron garnet (YIG), gadolinium gallium garnet (GGG), yttrium gallium garnet (YGG), etc. is already attempted through combustion synthesis,[12−15] and it needs further attention to extend the use of this technique to synthesize other important materials of this family also.

Excellent optical features of the garnets are derived from lanthanide ions doped in them. Lanthanide ions possess ladder like energy levels and hence multimode emission processes, i.e., downshifting (a normal photoluminescence process which involves transformation of one absorbed high-energy photon into one lower-energy photon), upconversion (a nonlinear process in which low energy photons are used to generate high

Received: April 11, 2014
Published: August 27, 2014

   dx.doi.org/10.1021/ic500854k | *Inorg. Chem.* 2014, 53, 9561−9569

energy photons, usually infrared excitation source), and quantum cutting (a process which transforms the energy of one higher energy photon into two (or more) lower energy photons), are possible in certain lanthanide doped materials. Multimodal emission is quite promising for many different applications including bioimaging and energy harvesting (solar cell) and was recently reported in fluoride, oxide, and a few other hosts.[16−18] Remarkably, UC and QC both are best achieved in a low phonon frequency host so fluorides are widely explored. However, multimodal emission is not well reported in garnet phosphor, except the YAG host of this family. There are several articles which report DS and UC independently in garnets.[4,5,8,9,19−21] However, only a few reports are available for QC; moreover, all of them have been carried out in a YAG host.[22−26] To the best of our knowledge, QC is not investigated in the yttrium gallium garnet (YGG) host, which produces a new insight for this subject to explore in details. Particularly, the QC process which can convert one short wavelength radiation (ultraviolet/visible) into two or more near-infrared (NIR) emissions around 1000 nm is of great interest, since the conversion efficiency of c-Si solar cells is paramount in the 950−1100 nm spectral region, while it is very poor in the ultraviolet/visible region.[27]

In light of the above requirements, the present work aims to explore a new perspective (i.e., low temperature synthesis, development of nanostructure, and ability to exhibit multimode luminescence) in garnets. For this purpose, we have synthesized Tb^{3+} and Yb^{3+} codoped YGG phosphor using a low temperature solution combustion technique, which is unique in the sense that we have explored the different outcome of this low temperature synthesis technique such as removal of fluorescence quenching entities, the presence of a minor secondary phase, existence of minor secondary phase even up to 1400 °C post annealing temperature, etc. The terbium(III) ion has been selected as an activator because of its capability to emit through all three processes (in the presence of Yb^{3+}), i.e., UC, QC, and DS. In addition to this, the QC mechanism ($Tb^{3+} \rightarrow Yb^{3+}$) would be favorable in the case of crystalline silicon solar cells.

The strategy of spectral conversion for multimodal emission (with representative partial energy level scheme) for the present YGG phosphor is shown in Figure 1. There is a broad excitation range, from 250 to 500 nm, arising due to both host and dopant ions, and the discrete emission is obtained in the entire visible region (blue, green, and red) through DS and QC processes. NIR photons are converted to visible photons via a frequency UC process. The ytterbium(III) ion acts as a sensitizer for the terbium emission during the UC process. The present studies reveal that the garnet phosphor could be very useful in display devices, enhancing the conversion efficiency of next generation solar cells etc.

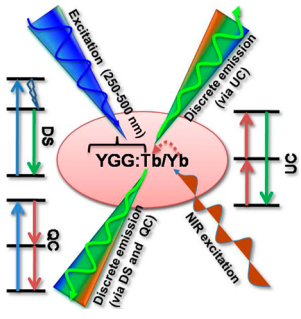

Figure 1. Schematic illustration to achieve multimodal luminescence through upconversion (UC), downshifting (DS), and quantum cutting (QC) processes in Tb^{3+}/Yb^{3+} codoped YGG phosphor. NIR stands for near-infrared.

2. EXPERIMENTAL SECTION

2.1. Materials and Synthesis. Analytical reagent (AR) grade yttrium nitrate ($Y(NO_3)_3{\cdot}6H_2O$, 99.9%, Molychem), gallium nitrate ($Ga(NO_3)_3{\cdot}H_2O$, 99.99%, Alfa Aeasar), terbium oxide (Tb_4O_7, 99.9%, Alfa Aeasar), ytterbium oxide (Yb_2O_3, 99.9%, Loba Chemie), nitric acid (99.9%, Merck), and urea (Loba Chemie) were used for synthesis of the material. YGG phosphors were synthesized according to $Y_{3-x-y}Tb_xYb_yGa_5O_{12}$ (x = 0.000, 0.005, 0.008, 0.01, 0.012, 0.015 and y = 0.00, 0.03, 0.05, 0.10, 0.15) compositional formula.

The phosphor was prepared using a solution combustion technique.[28] This synthesis process involves an exothermic reaction in which metal nitrate acts as an oxidizing agent while urea acts as an organic fuel (reducing agent). The mixture of nitrates and urea was stirred in a beaker for 2 h to get a homogeneous solution. The solution was then heated at 60 °C to evaporate water. As the water content in the solution is decreased, the solution changes to a transparent gel. The gel was then transferred into a platinum crucible and kept in a closed furnace maintained at 650 °C. Auto-ignition takes place within a few minutes, which results in a voluminous and foamy product. Further, the obtained product was grinded in an agate mortar to get fine powders. The synthesized sample was then post annealed at 800 °C for 4 h to improve crystallinity and to reduce luminescence quenching centers from as-synthesized phosphor, as is clear in Fourier transform infrared (FTIR) measurement.

2.2. Characterization. FTIR spectroscopic measurements were carried out on a Thermo Scientific FTIR spectrometer (model: NICOLET 6700). Spectra were collected at a resolution of 2 cm^{-1}, and each spectrum was an average of 32 scans. Phase identification was carried out using an 18 kW Cu rotating anode based high resolution Rigaku X-ray powder diffractometer (XRD) fitted with a curved crystal monochromator in a diffracted beam. Data were obtained from 2θ = 10° to 80° at a scanning speed of 3°/min. Phosphor was investigated by high resolution transmission electron microscopy (HRTEM, Technai, Model: G20-twin, 200 kV) to explore microstructural information as well as for the demonstration of lattice fringes to evaluate the quality of crystals. For HRTEM, a powder sample was dispersed in ethanol by sonication, and a drop of liquid was placed over a copper grid and was left undisturbed until it became dry.

For UC measurement, 976 nm radiation from a diode laser (2W, continuous mode, power tunable, Model-III980, Chengchun New Industries optoelectronics tech. Co. Ltd.) was used to excite the samples, while an iHR320 (Horiba Jobin Yvon) monochoromator equipped with a photomultiplier tube (PMT, R928) was used to disperse and detect the signal. Photoluminescence excitation (PLE) and emission (PL) measurements were performed using a Fluorolog-3 spectrofluorometer (Model: FL3−11, Horiba Jobin Yvon) equipped with 450 W xenon flash lamp. To estimate the absolute luminescence quantum efficiency of the QC phosphors, an integrating sphere equipped with an Edinburgh spectrometer (model F900) instrument has been used, and then by measuring the integrated fraction of luminous flux and radiant flux with the standard method, quantum efficiency has been evaluated. The lifetime measurements were performed using a pulsed xenon lamp (25 W) attached with the Fluorolog-3 spectrofluorometer. The PMT used in the spectrofluorometer has its higher detection limit at 850 nm. Therefore, the 266 nm excitation wavelength of a Nd:YAG laser (Innolas, Spitlight 600) and CCD (charged coupled device) detector (Ocean Optics, QE 65000) was used for QC measurement.

3. RESULTS AND DISCUSSION

3.1. Fourier Transform Infrared (FTIR) Measurement. The use of organic material (urea) as fuel during the synthesis

dx.doi.org/10.1021/ic500854k | Inorg. Chem. 2014, 53, 9561−9569

of phosphor makes it imperative to search for the presence of high vibrational bands responsible for fluorescence quenching.[28] FTIR spectra of the as-synthesized sample and the sample annealed at 800 °C for 4 h are shown in Figure 2. The

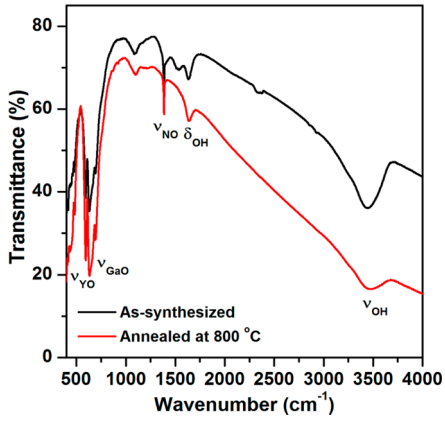

Figure 2. Fourier transform infrared (FTIR) spectra of $Y_{2.96}Tb_{0.01}Yb_{0.03}Ga_5O_{12}$ phosphor, as-synthesized and annealed at 800 °C/4 h.

spectrum of as-synthesized phosphor sample shows characteristic bands corresponding to OH, NO, NO_3^-, and CO_3^{2-} groups. A broad peak centered at 3442 cm^{-1} is due to symmetric stretching vibrations of the hydroxyl group (υ_{OH}). Another broad peak near 1638 cm^{-1} is also due to the bending modes of the hydroxyl group (δ_{OH}).[29] A broad peak due to the stretching vibration of NO (υ_{NO}) appears around 1384 cm^{-1}. The surface adsorbed NO_3^- group is responsible for this quenching entity.[29] The intensity of these peaks decreases significantly as the sample is post annealed at higher temperature. The other vibration bands, due to the inorganic/metallic bonds of host lattice (Y−O, Ga−O vibrations), are observed in the 400−700 cm^{-1} range.[30] Since the luminescence quenching centers are reduced significantly in annealed powder (at 800 °C for 4 h), further studies were carried out on an annealed sample.

3.2. Structural Characterization: X-ray Diffraction, Le Bail Refinement, and Transmission Electron Microscopy.

X-ray diffraction patterns of pure and lanthanide doped garnet phosphors were recorded to identify the phase composition and crystal structure (see Supporting Information, Figure S1). The XRD peaks in pure and lanthanide doped YGG phosphors are found to be almost identical, which suggests that Tb^{3+} ions replaced Y^{3+} ions in the lattice effectively. There are few additional low intensity peaks in the X-ray diffraction pattern of the YGG phosphor which could not be indexed using *Ia*3*d* space group of the cubic cell which is a well-known structure of YGG phosphor (see inset of Figure 3a).[31] The low intensity peaks occur due to another secondary minor phase of Y_3GaO_6 (~7% in total) which is formed because of the deficiency of gallium in the sample. As it is well-known that during the combustion synthesis process, the flame temperature reaches up to 1400 ± 100 °C,[32] we believe that some of the gallium is evaporated during the combustion synthesis process. In order to index the low intensity XRD peaks, we determine the space group and unit cell parameters of the Y_3GaO_6 phase by Le Bail fitting of the XRD data using the "FULLPROF" refinement program.

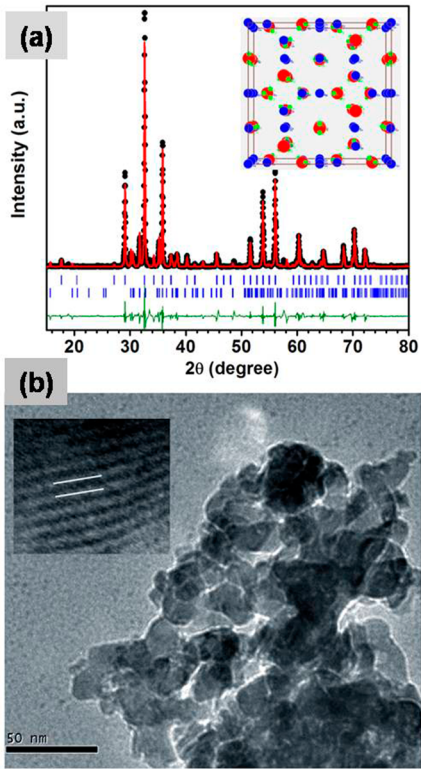

Figure 3. (a) Observed (dots), calculated (continuous line), and difference (bottom line) profiles obtained after Le Bail fit for YGG phosphor using *Ia*3*d* space group (of cubic cell) for $Y_3Ga_5O_{12}$, and $Cmc2_1$ space group (of orthorhombic cell) for Y_3GaO_6 phases. Vertical tick marks above the difference plot show the positions of the Bragg peaks. The inset shows the crystal structure of YGG, blue balls are for Ga, red for Y, and green balls are for O. (b) Transmission electron microscopy (TEM) image of YGG phosphor. The inset shows the lattice fringes, indicating a high crystal quality with minimal lattice fringe distortions.

The refinement was carried out using a two phase model; for $Y_3Ga_5O_{12}$ and Y_3GaO_6 phases, the peak profiles were defined by Pseudo-Voigt function, and the background was described in terms of a six coefficient polynomial. A very good fit is observed by considering the *Ia*3*d* space group (cubic cell) for $Y_3Ga_5O_{12}$ and $Cmc2_1$ space group (orthorhombic cell) for $Y_3Ga_5O_{12}$ phases with the lattice parameter $a = b = c = 12.2705(5)$ Å, and $a = 9.0443(2)$, $b = 11.2726(5)$, $c = 5.4637(3)$ Å, respectively (see Figure 3a), confirm the $Cmc2_1$ space group of Y_3GaO_6 phase. In order to get phase pure YGG phosphors, we annealed the samples at different temperatures (XRD pattern shown in Figure 4). But even at 1400 °C annealing, there was no change in the XRD patterns. A similar observation is also made by Krsmanovic et al. for GGG (gadolinium gallium garnet) material synthesized by solution combustion route.[14] The microstructure analysis has also been done by using TEM measurement (see Figure 3b). TEM clearly depicts the formation of nanocrystals of average diameter lying in the range of 20−30 nm. The shape of the particles is less homogeneous; however, most of the particles are nearly spherical. Some of the particles are lacking in clear grain boundary and show an agglomerated type of structure. In the inset of Figure 3b, clear and damage-free lattice fringes are easily observed which reveal a good crystal quality with minimal lattice fringe distortion.

dx.doi.org/10.1021/ic500854k | Inorg. Chem. 2014, 53, 9561−9569

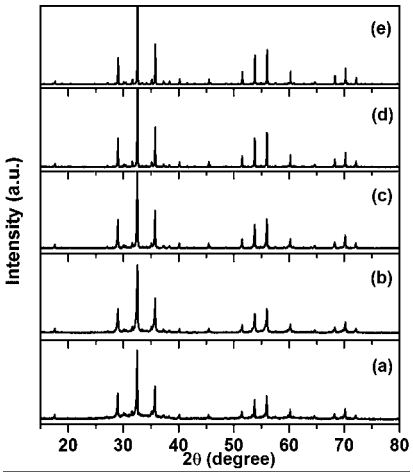

Figure 4. X-ray diffraction patterns of $Y_{2.96}Tb_{0.01}Yb_{0.03}Ga_5O_{12}$ phosphors: (a) as-synthesized, (b) annealed at 800 °C/4 h, (c) annealed at 1000 °C/4 h, (d) 1200 °C/4 h, and (e) annealed at 1400 °C/4 h.

3.3. Multimodal Luminescence Process. Trivalent lanthanide ions are well-known to exhibit efficient visible emission by DS, QC, and UC processes. Each process has certain typical requirements, and so, until now, there are few rare reports which cover all the luminescence mechanisms in a single host matrix until date. Recently, the subject has emerged as a hot research topic in lanthanide based phosphors owing to their multifunctional behavior, besides the well established lamp and display applications, viz., for multimodal imaging, fluorescence labeling, and in the enhancement of the conversion efficiency of silicon solar cells etc.[8,9,33]

3.3.1. Upconversion (UC): Infrared to Green UC Emission through Cooperative Sensitization of Yb^{3+} Ions. UC study of YGG has been done with IR radiation (976 nm). The $^5D_4$ level of the Tb^{3+} ion lies at ~20 400 cm^{-1}, which is ~14 000 cm^{-1} above to the uppermost ground multiplet, i.e., $^7F_0$. There is no level of Tb^{3+} ion in between. Thus, under the 976 nm (~10 000 cm^{-1}) excitation, the possibility for UC solely due to Tb^{3+} is not feasible. Consequently, Tb^{3+} doped YGG samples do not emit any radiation on 976 nm excitation. However, Yb^{3+}, a well-known efficient absorber of 976 nm radiation, can give a cooperative emission (~20 000 cm^{-1}) by the involvement of the Yb^{3+}–Yb^{3+} ion pair.[34] This energy may be transferred to the $^5D_4$ level of Tb^{3+}, which could open the possibility for UC emission from the Tb^{3+} ion. Therefore, $Y_{2.89}Tb_{0.01}Yb_yGa_5O_{12}$ phosphors (where y = 0.03, 0.05, 0.10, 0.15) were synthesized to achieve the UC emission. It is clear from the right inset to Figure 5a that maximum UC is at 10 mol % of Yb^{3+}, and beyond this concentration, UC begins to decrease due to the concentration quenching effect at higher concentrations. Figure 5a shows the room temperature UC emission spectrum of the $Y_{2.89}Tb_{0.01}Yb_{0.10}Ga_5O_{12}$ phosphor on excitation with 976 nm. The UC emission spectrum shows characteristic peaks of the Tb^{3+} ion peaking at 485, 489, 544, 592, 626, 656, and 676 nm owing to the electronic transitions $^5D_4 \rightarrow {}^7F_6$, $^5D_4 \rightarrow {}^7F_5$, $^5D_4 \rightarrow {}^7F_4$, $^5D_4 \rightarrow {}^7F_3$, $^5D_4 \rightarrow {}^7F_2$, and $^5D_4 \rightarrow {}^7F_1$, respectively. The $^5D_4 \rightarrow {}^7F_5$ transition (at 544 nm) appears with maximum intensity, and thus the overall emission appears with a green tinge. Few weak transitions in the ultraviolet (UV)/blue region, i.e. at 408, 419, and 437 nm, correspond to $^5D_3 \rightarrow {}^7F_6$, $^5D_3 \rightarrow {}^7F_5$, and $^5D_3 \rightarrow {}^7F_4$ transitions, respectively also appear, see left inset to Figure 5a.

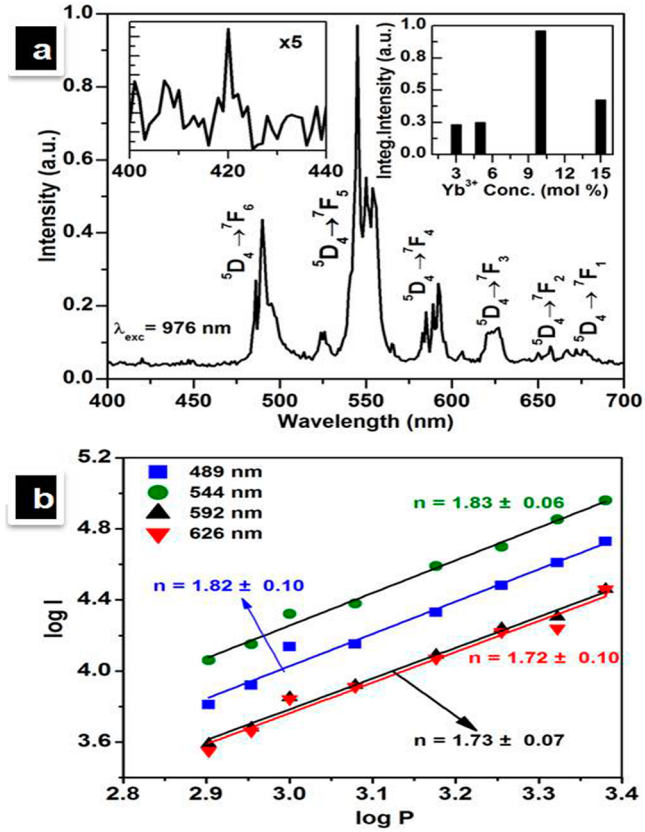

Figure 5. (a) Room temperature upconversion spectrum of $Y_{2.89}Tb_{0.01}Yb_{0.10}Ga_5O_{12}$ phosphor in the range 400–700 nm on excitation with 976 nm radiation. Left inset shows the enlarged portion of the emission spectrum in the 400–450 nm range, and inset ii shows the integrated intensity of green emission with respect to different concentrations of Yb^{3+}. (b) Effect of laser input power on the emission intensity of different transitions in $Y_{2.89}Tb_{0.01}Yb_{0.10}Ga_5O_{12}$ phosphor under 976 nm excitation. The slope of the plot gives the involvements of a number of photons in the particular upconversion transition.

In the low power regime, the UC phenomenon follows the nonlinear relationship: $I_{UC} \propto P^n$, where I_{UC} is the UC emission intensity, P is the excitation power, and n is the number of photons needed to produce the fluorescence; however, this relation is not always true, and this relation changes at high pump power.[35,36] Thus, by getting the value of n, one can support the UC mechanism proposed. Power dependence study of the upconverted emissions from Tb^{3+} ions are shown in Figure 5b. This study shows the quadratic dependence of the intensity of blue, green, and red emissions on the pump power. This means that two photons of 976 nm are required for the population buildup in the $^5D_4$ level. This study further confirms the proposed mechanism for the different upconverted emissions from $Y_{2.89}Tb_{0.01}Yb_{0.10}Ga_5O_{12}$ phosphor.

The complete UC mechanism involved in the process is shown schematically in Figure 6 (partial energy level diagram). The cooperatively excited Tb^{3+} ions in the $^5D_4$ level, due to the involvement of Yb^{3+} ion pair through CET (cooperative energy transfer), give upconverted strong green and relatively weak blue and red emissions. Further, the $^5D_3$ level can be populated when few Tb^{3+} ions in the $^5D_4$ level reabsorb the incident 976 nm photons and are promoted to higher lying excited states

dx.doi.org/10.1021/ic500854k | Inorg. Chem. 2014, 53, 9561–9569

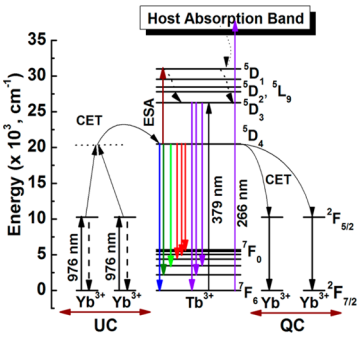

Figure 6. Schematic energy level diagram of Tb^{3+} and Yb^{3+} showing the mechanism involved in various upconversion (UC) transitions, downshifting, and quantum cutting (QC). CET stands for cooperative energy transfer.

($^5D_1$) through a process known as excited state absorption (ESA). Another pathway to populate this level is the nonradiative energy transfer from one excited Yb^{3+} ion. Then, after, the $^5D_3$ level is populated through a nonradiative process, and emissions in UV/blue are observed.[37]

3.3.2. Downshifting (DS): Photoluminescence Excitation (PLE), Emission (PL), and Decay Dynamics. The excitation spectra of Tb^{3+} doped YGG ($Y_{2.99}Tb_{0.01}Ga_5O_{12}$) phosphor were obtained by monitoring the emission of Tb^{3+} for the $^5D_4 \rightarrow {}^7F_5$ (at 541 nm) and $^5D_4 \rightarrow {}^7F_6$ (at 487 nm) transitions, shown in Figure 7a. It is evident from the excitation spectra that there are two important regions. Both the excitation spectra consist of a few broad bands, toward the shorter wavelength side, and several sharp excitation peaks on the other side of the spectrum. Two broad peaks are observed with a maximum at 283 and 310 nm in the 250−330 nm regime, which could be assigned due to the absorption band of the YGG host (i.e., host absorption band).[38] The f−d transitions of Tb^{3+} ions are also known to appear in this region. Since, f−d transitions are allowed transitions; they are expected to arise with higher intensity compared to the f−f transition of Tb^{3+} ion. However, here, f−f transitions of Tb^{3+}, appearing mostly in 325−500 nm, are more intense than broad bands. From this, we conclude that, in the YGG host, the broad bands are arising due to the contribution of both the absorption band of the host as well as the f−d transition of Tb^{3+} ion. Similar result has been reported in GGG phosphor by Rodríguez et al.[39]

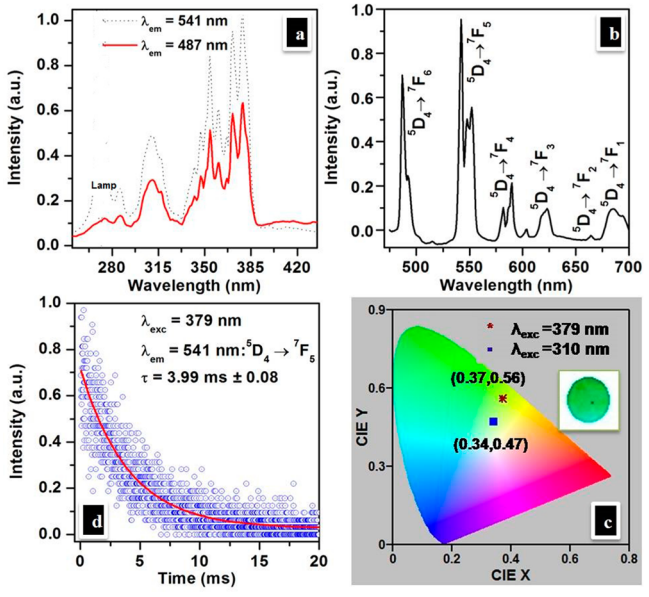

Figure 7. (a) Excitation spectra of $Y_{2.99}Tb_{0.01}Ga_5O_{12}$ phosphor observed by monitoring the emission at 541 and 487 nm corresponding to $^5D_4 \rightarrow {}^7F_5$ and $^5D_4 \rightarrow {}^7F_6$ transitions of Tb^{3+} ion. (b) Room temperature photoluminescence spectra of $Y_{2.99}Tb_{0.01}Ga_5O_{12}$ phosphor (annealed at 800 °C/4 h) on excitation with 379 nm radiation. (c) CIE chromaticity diagram showing the color coordinates for green color perception of the emission in $Y_{2.99}Tb_{0.01}Ga_5O_{12}$ phosphor and the inset shows the digital photograph of the green emission. (d) Decay curve showing a monoexponential fitting (in red) for 541 nm emission corresponding to $^5D_4 \rightarrow {}^7F_5$ transition under 379 nm excitation.

Figure 7b shows the emission spectrum of $Y_{2.99}Tb_{0.01}Ga_5O_{12}$ phosphor (λ_{exc} = 379 nm). The spectrum contains different emissions at 487, 541, 590, 624, 665, and 685 nm corresponding to $^5D_4 \rightarrow {}^7F_6$, $^5D_4 \rightarrow {}^7F_5$, $^5D_4 \rightarrow {}^7F_4$, $^5D_4 \rightarrow {}^7F_3$, $^5D_4 \rightarrow {}^7F_2$, and $^5D_4 \rightarrow {}^7F_1$ transitions, respectively. The green emission due to $^5D_4 \rightarrow {}^7F_5$ transition of the Tb^{3+} ion is the dominant one among all the emissions. Excitation at 379 nm directly populates the $^5D_3$ level of the Tb^{3+} ion. The excited ions relax to the $^5D_4$ level through nonradiative channels. Finally, the radiative emissions in blue, green, and red regions are observed from the $^5D_4$ level. Excitation with other suitable wavelengths (e.g., 310 nm) also gives a similar result, except a variation in the emission intensity of different bands (see Supporting Information Figure S2).

In order to study the effect of Tb^{3+} ion concentrations on luminescence intensity, we synthesized $Y_{3-x}Tb_xGa_5O_{12}$ phosphor for x = 0.005, 0.008, 0.01, 0.012, and 0.015. It was found that luminescence for green emission is optimum at 1.0 mol % Tb^{3+} ($Y_{2.99}Tb_{0.01}Ga_5O_{12}$), and it is shown in Supporting Information Figure S2. Comparison has been made by taking the integrated intensity of the dominant green emission for all the samples. In our case, luminescence from a higher excited $^5D_3$ state is very weak, showing that almost all the population is being accumulated in the $^5D_4$ level, thereby giving dominant green emission. Concentration quenching can be explained on the basis of energy migration among the activator ions. In this process, the excitation energy will be lost at a killer or quenching site, resulting in the decrease in emission intensity.

The color perception corresponding to luminescence from different samples was also estimated. Color perception is a psychophysical property of the human eye, and this response can mathematically be expressed well in terms of CIE coordinates given by the International Commission for

dx.doi.org/10.1021/ic500854k | Inorg. Chem. 2014, 53, 9561−9569

Illumination (CIE, Commission Internationale de l'Eclairage).[28] It involves parameters x and y to specify the chromaticity, which covers the properties hue and saturation on a two-dimensional curve, known as chromaticity diagram. The chromaticity coordinates were calculated for $Y_{2.99}Tb_{0.01}Ga_5O_{12}$ sample at 379 and 310 nm excitation wavelengths, shown in Figure 7c. The coordinates obtained are (0.37, 0.56) and (0.34, 0.47), respectively which are reasonably good for different optical applications.

The decay curve of the emission wavelength at 541 nm was recorded under the 379 nm excitation wavelength to have an idea about the lifetime of the level involved in green transition. The lifetime associated with a transition from higher level to a lower level is defined as the time duration in which the population of the higher level reduces by 1/e times of its initial population. Thus, the measured lifetime of a particular level is determined by taking first e-folding time of the decay curve. So the data for decay curve was fitted to the following equation

$$I = I_0 \exp\left(-\frac{t}{\tau}\right) \quad (1)$$

where τ is the lifetime of the emitting level. Figure 7d shows the room temperature decay curve for $^5D_4 \rightarrow {}^7F_5$ transition. The curve fitting of the decay profile was found to be single exponential, and the decay time thus obtained for the $^5D_4$ excited state is $\tau \sim 3.99$ ms. This is consistent with the data reported earlier for this transition.[39]

Interestingly, the PL and PLE spectra show a decrease in emission intensity with a variation in the Yb^{3+} concentration. This was also clear in the absolute luminescence quantum efficiency (η_{QE}) measurement of the DS emission with a variation in Yb^{3+} concentration. Maximum efficiency is obtained for the Yb^{3+} undoped sample ($Y_{2.99}Tb_{0.01}Yb_{0.00}Ga_5O_{12}$), i.e., η_{QE} = 71 ± 1.6%, and then a gradual decrease is observed for 3 mol % (η_{QE} = 64 ± 1.9%), 5 mol % (η_{QE} = 61 ± 1.7%), 10 mol % (η_{QE} = 54 ± 1.5%), and 15 mol % (η_{QE} = 43 ± 1.4% %). However, on the other hand, a structured emission peaking in the range 900−1040 nm is observed (see Figure 8), which shows an increase in intensity with increasing concentration of Yb^{3+}. This was not possible to explain by simple downshifting emission of Tb^{3+}, as it does not have any level to give emission in the near-infrared regime (first excited state lies above 20 000 cm^{-1}). Moreover to that, the codoped Yb^{3+} ions are also not being excited directly by a UV radiation (379 nm in this case) source, as the uppermost excited state for Yb^{3+} lies ∼10 000 cm^{-1} only. So, the only possibility seems to be the quantum cutting (QC) emission of Yb^{3+} ions. This is further explored in the next section.

3.3.3. Quantum Cutting (QC). The phenomenon of QC generates two or more low energy (visible/IR) photons after the absorption of a high energy photon (VUV (vacuum ultraviolet)/UV/visible) by the luminescent materials. QC was first observed in Pr^{3+}:YF_3 during the 1970s. Nowadays, research is focused on the observation of QC process based on the concept of the dual ions doped materials, one acting as donor and the other as acceptor. The energy transfer assisted relation to obtain QC is also known as DC (contrary to the UC phenomenon), which is further divided into two categories based on the type of energy transfer involved. First order DC is based on the resonant energy transfer, which requires a good overlap between the emission spectrum of the donor and the excitation spectrum of the acceptor ion. While the second order DC phenomenon accounts for the nonresonant energy transfer

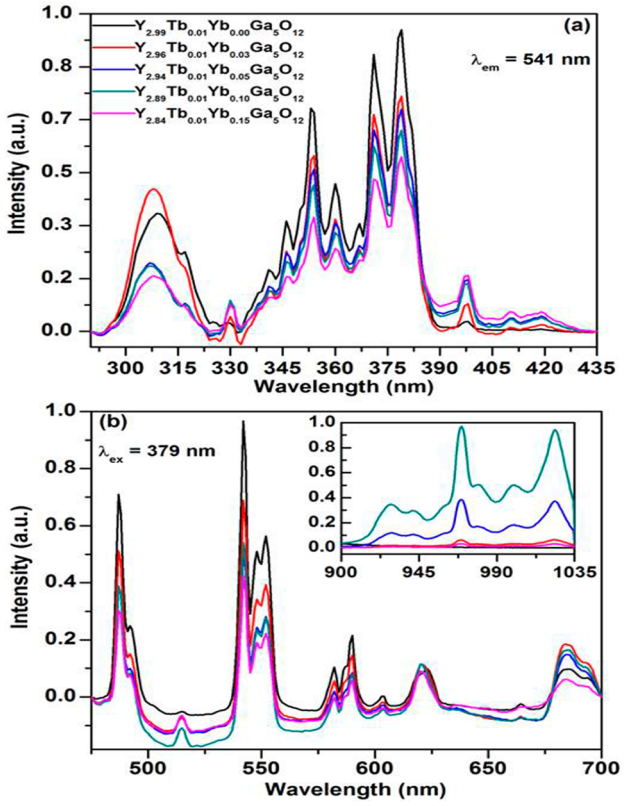

Figure 8. (a) Room temperature photoluminescence excitation spectra (λ_{em} = 541 nm for $^5D_4 \rightarrow {}^7F_5$ transition) and (b) emission spectra (λ_{ex} = 379 nm) of the Tb^{3+} ion at different concentrations of the Yb^{3+} ion. Inset shows the NIR emission spectrum of the Yb^{3+} ion through the QC process.

due to a mismatch between emission and excitation spectra of donor and acceptor ions. Unlike the first order DC, in this case the donor excites two acceptor ions simultaneously (cooperative sensitization). QC have been studied mostly in fluoride hosts as they possess wide gap and low phonon energy suitable for this purpose. However, chemical instability and high toxicity limit their applications, and so oxides are preferred. Oxides show many distinguished characters such as high stability, high VUV absorption cross-section, easy fabrication, economic, etc. Recently, researchers are looking forward to utilize these phosphors for energy harvesting, e.g. in solar cell research. The conventional solar cells based on crystalline Si (Eg = 1.1 eV) shows significant energy loss due to the thermalization of electron−hole pairs (generated by the absorption of high energy photons).[40] The lacunae can be resolved to an extent by using these QC phosphors.

Keeping this idea in mind, authors tried to check the QC phenomenon in the present system. Figure 8 shows the emission spectra of $Y_{(2.99-y)}Tb_{0.01}Yb_yGa_5O_{12}$ (y = 0.00, 0.03, 0.05, 0.10, 0.15) phosphor (λ_{ex} = 379 nm). The spectra contain the characteristic visible emissions with a gradual decrease in visible emission intensity with an increase in the concentration of Yb^{3+}. However, there is an increase in NIR emission intensity with maximum for $Y_{2.89}Tb_{0.01}Yb_{0.10}Ga_5O_{12}$. But the emission in the NIR region does not belong to the Tb^{3+} ion because there is no energy level corresponding to the NIR region (the difference between the uppermost level of ground multiplet and the first excited state for Tb^{3+} is almost 14 000 cm^{-1}), so the NIR transition cannot be explained due to the Tb^{3+} ion. The

dx.doi.org/10.1021/ic500854k | Inorg. Chem. 2014, 53, 9561−9569

UC discussed earlier is obtained by the second order CET from two Yb^{3+} ions to one Tb^{3+} ion on the basis of the energy match relationship. In the same way, a CET from Tb^{3+} to two Yb^{3+} ions is also plausible (see Figure 6), i.e.

$$Tb^{3+}(^5D_4) \rightarrow 2Yb^{3+}(^2F_{5/2})$$

Thus, the emission in the NIR region (900−1040 nm) is assigned to the transitions of Yb^{3+} from the different Stark levels of $^2F_{5/2}$ multiplet to the different Stark levels of $^2F_{7/2}$ multiplet. The resonant energy transfer from one Tb^{3+} to one Yb^{3+} is not possible because the Yb^{3+} ion has only one excited multiplet ($^2F_{5/2}$) ∼ 10 000 cm^{-1}, and there is no energy level of Tb^{3+} ion situated in this energy region. This trend suggests the possibility of transfer of excitation energy of the Tb^{3+} ion to Yb^{3+} ions, which results in the observed NIR emission. It is to be mentioned here that NIR emission due to the Yb^{3+} ion ($^2F_{5/2} \rightarrow {}^2F_{7/2}$) was monitored with 266 nm a from Nd:YAG laser and CCD detector (with detection limit ∼1060 nm) since the PMT attached with the spectrofluorometer is limited to 850 nm detection. The decrease in NIR emission beyond 10 mol % of Yb^{3+} may be due to concentration quenching or energy migration among nearby Yb^{3+} ions at higher concentration. Thus, with increasing concentration of Yb^{3+}, a decrease in the intensity of the peaks of Tb^{3+} ion and, contrary to this, an increase in the intensity of the emission peak of Yb^{3+} clearly supports an energy transfer from Tb^{3+} to Yb^{3+}, which is possible via a QC process. Strek et al. have also verified a simultaneous energy transfer mechanism from one Tb^{3+} to two different Yb^{3+} ions in $KYb(WO_4)_2$ matrix.[41]

Thus, the complete mechanism is as follows: as discussed in section 3.3.1, the bands in 250−330 are assigned to the host absorption and f−d transitions of Tb^{3+}. Therefore, authors have proposed one mechanism that, when $Y_{2.96}Tb_{0.01}Yb_{0.03}Ga_5O_{12}$ phosphor is exposed with UV (266 nm) light, the absorption band of the host matrix is excited. Further, this excitation energy is transferred to the Tb^{3+} ion through nonradiative relaxation, and finally the $^5D_3$ and $^5D_4$ levels are populated. The $^5D_3$ and $^5D_4$ levels are populated also due to f−d excitation and usual relaxation processes. The different emissions from excited $^5D_3$ and $^5D_4$ (Tb^{3+}) to ^7F_j (j = 6, 5, 4, 3, 2, 1) are observed in the near UV and visible regions. This type of host sensitized energy transfer to lanthanide ions is obtained in other hosts also.[42] However, a part of $^5D_4$ population is transferred to two different Yb^{3+} ions simultaneously, and as a result NIR emissions are obtained from the Yb^{3+} ion through a cooperative QC process.

In order to further verify the QC process, the decay curve analysis for the samples doped with varying concentrations of Yb^{3+} has been carried out. Figure 9 presents the decay curve behavior of Tb^{3+} ion for the $^5D_4 \rightarrow {}^7F_5$ transition at different concentrations of Yb^{3+} (well fitted to eq 1). Data clearly show the continuous decrease in the lifetime of the Tb^{3+} ion with an increase in concentration of Yb^{3+}. It decreases from 3.99 ms (0 mol % Yb) to 2.91 ms (15 mol % Yb). Also, the photoluminescence measurement shows the same trend. Therefore, the CET from Tb^{3+} to Yb^{3+} is proposed, and the energy transfer efficiency can be calculated from the eq:

$$\eta_{ET} = 1 - \frac{\tau_x}{\tau_0} \quad (2)$$

where τ_x and τ_0 are the fluorescence lifetime of Tb^{3+}/Yb^{3+} and singly Tb^{3+} doped phosphors, respectively. The value of η_{ET} estimated for different concentrations of Yb^{3+} using the above relation is given in Table 1. It is obvious from the data in Table 1 that ET efficiency increases with increasing the Yb^{3+} concentration, and reaches to a maximum of 28% for 15 mol % of Yb^{3+} concentration. The internal quantum efficiency (QE) of the phosphor samples, can be calculated by

$$\eta_{QE} = \eta_{Tb}(1 - \eta_{ET}) + 2\eta_{ET} \quad (3)$$

The first term in the relation belongs to the visible photons emitted by Tb^{3+} ions, and the second term refers to the NIR photons emitted by Yb^{3+} ions. Here, η_{Tb} represents the quantum efficiency of the emission of Tb^{3+} ions. Ignoring the nonradiative transitions (i.e., η_{Tb} = 1), the highest possible QE is 128% for $Y_{2.84}Tb_{0.01}Yb_{0.15}Ga_5O_{12}$ phosphor. This means absorption of each 100 photons (of 266 nm radition) produces a total of 128 photons (NIR and visible both), out of which 56 photons are emitted in 900−1040 nm (NIR) while the rest of the 72 photons are emitted in visible region. The calculated value of the internal QE is increased notably with increment of the Yb^{3+} concentration (see Table 1). This is the first report on QC in a YGG host to the best of our knowledge. Thus, this garnet phosphor can be a promising material in many applications including its application in increasing the conversion efficiency of solar cells.

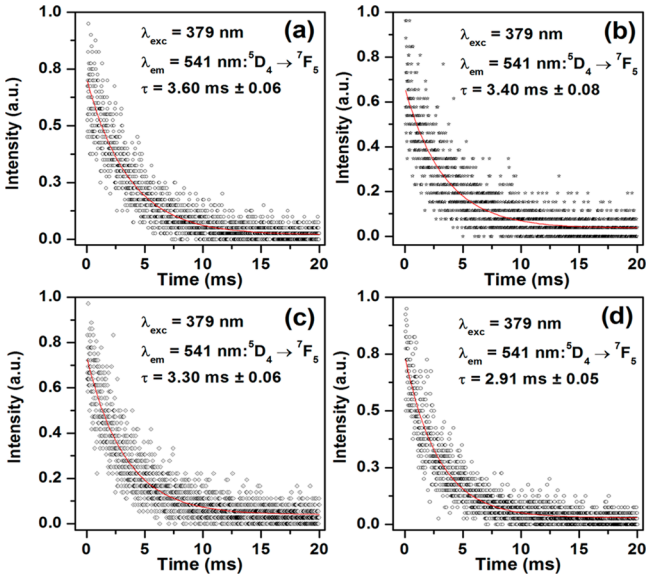

Figure 9. Decay curve measurement of (a) $Y_{2.96}Tb_{0.01}Yb_{0.03}Ga_5O_{12}$, (b) $Y_{2.94}Tb_{0.01}Yb_{0.05}Ga_5O_{12}$, (c) $Y_{2.89}Tb_{0.01}Yb_{0.10}Ga_5O_{12}$, (d) $Y_{2.84}Tb_{0.01}Yb_{0.15}Ga_5O_{12}$.

Table 1. Estimated Values of Energy Transfer Efficiency (η_{ET}) and Internal Quantum Efficiency (η_{QE}) of Tb^{3+}:YGG Phosphors with Varying Concentration of Yb^{3+}

sample	τ (ms)	η_{ET} (%)	η_{QE} (%)
$Y_{2.99}Tb_{0.01}Yb_{0.00}Ga_5O_{12}$	3.99	0	100
$Y_{2.96}Tb_{0.01}Yb_{0.03}Ga_5O_{12}$	3.60	10	110
$Y_{2.94}Tb_{0.01}Yb_{0.05}Ga_5O_{12}$	3.40	15	115
$Y_{2.89}Tb_{0.01}Yb_{0.10}Ga_5O_{12}$	3.30	18	118
$Y_{2.84}Tb_{0.01}Yb_{0.15}Ga_5O_{12}$	2.91	28	128

dx.doi.org/10.1021/ic500854k | Inorg. Chem. 2014, 53, 9561−9569

4. CONCLUSION

In conclusion, Tb^{3+}/Yb^{3} codoped yttrium gallium garnet (YGG) nanophosphors have been successfully synthesized by the solution combustion method. The method shows the advantages of synthesis at low temperature, homogeneous composition, development of fine grains of the order of nanosize, etc. when compared to the solid state reaction method. Structural characterization reveals the formation of $Y_3Ga_5O_{12}$ (major) and Y_3GaO_6 (minor, secondary) phases. Material shows a wide excitation feature ranging from 250 to 500 nm and emits in the green region through DS and UC processes, while NIR emission of ∼1000 nm is observed through a QC ($Tb^{3+} \rightarrow Yb^{3+}$) process. These excitation and emission characteristics are highly favorable for phosphor coated c-Si solar cell applications. The energy transfer from Tb^{3+} to Yb^{3+} has been verified with efficiency as high as 28%, and corresponding quantum efficiency of QC are calculated to be 128%. This confirms the first time observed multimodal emission behavior of yttrium gallium garnet phosphor, which legitimates many potential applications of this material.

■ ASSOCIATED CONTENT

Ⓢ Supporting Information

X-ray diffraction patterns of pure and lanthanide-doped YGG phosphors (Figure S1). Room temperature photoluminescence $Y_{2.99}Tb_{0.01}Ga_5O_{12}$ on excitation with different wavelengths based on the excitation spectrum and effect of Tb^{3+} concentration on the luminescence intensity of Tb^{3+}-doped yttrium gallium garnet phosphors (Figure S2). This material is available free of charge via the Internet at http://pubs.acs.org.

■ AUTHOR INFORMATION

Corresponding Author

*Tel.: +91-8574027822. Fax: +91 542 2369889. E-mail: sunilcfsl@gmail.com, sunilks.app@itbhu.ac.in.

Present Address

[#]Instituto de Ciencias Físicas, Universidad Nacional Autonoma de Mexico, Cuernavaca, Morelos C.P. 62210, México.

Notes

The authors declare no competing financial interest.

■ ACKNOWLEDGMENTS

S.K.S. thankfully acknowledges financial support by Department of Science and Technology (DST), New Delhi, India in the form of INSPIRE Faculty Award [IFA12-PH-21]. K.M. is thankful to CSIR, New Delhi for senior research fellowship (SRF). A.K.S. is thankful to DSK, PDF fellowship from UGC, New Delhi. The authors would like to thank DST, New Delhi for the research project.

■ REFERENCES

(1) Zhang, S. S.; Wang, Q. P.; Zhang, X. Y.; Cong, Z. H.; Fan, S. Z.; Liu, Z. J.; Sun, W. J. *Laser Phys. Lett.* **2009**, *6*, 864−867.

(2) Sato, Y.; Taira, T. *Opt. Mater. Exp.* **2012**, *2*, 1076−1087.

(3) Psuja P.; Hreniak, D.; Strek, W. Rare-Earth Doped Nanocrystalline Phosphors for Field Emission Display Application. *Photonics and Microsystems, 2006 International Students and Young Scientists Workshop, June 30−July 2 2006*; IEEE: Piscataway, NJ; Vol *50*, p 54.

(4) Birkel, A.; Denault, K. A.; George, N. C.; Doll, C. E.; Hery, B.; Mikhailovsky, A. A.; Birkel, C. S.; Hong, B. C.; Seshadri, R. *Chem. Mater.* **2012**, *24*, 1198−1204.

(5) Heer, S.; Wermuth, M.; Kramer, K.; Gudel, H. U. *Phys. Rev. B* **2002**, *65*, 125112/1−10.

(6) Papagelis, K.; Ves, S. *J. Phys. Chem. Solids* **2003**, *64*, 599−605.

(7) Malinowski, M.; Piramidowicz, R.; Frukacz, Z.; Chadeyron, G.; Mahiou, R.; Joubert, M. F. *Opt. Mater.* **1999**, *12*, 409−423.

(8) Chenais, S.; Druon, F.; Balembois, F.; Georges, P.; Brenier, A.; Boulon, G. *Opt. Mater.* **2003**, *22*, 99−106.

(9) Ferrand, B.; Chambaz, B.; Couchaud, M. *Opt. Mater.* **1999**, *11*, 101−114.

(10) Wang, M.; Mi, C. C.; Wang, W. X.; Liu, C. H.; Wu, Y. F.; Xu, Z. R.; Mao, C. B.; Xu, S. K. *ACS Nano* **2009**, *3*, 1580−1586.

(11) Shen, J.; Sun, L. D.; Yan, C. H. *Dalton Trans.* **2008**, *42*, 5687−5697.

(12) Huczko, A.; Kurcz, M.; Baranowski, P.; Bystrzejewski, M.; Bhattarai, A.; Dyjak, S.; Bhatta, R.; Pokhrel, B.; Kafle, B. P. *Phys. Status Solidi B* **2013**, *250*, 2702−2708.

(13) Vajargah, S. H.; Hosseini, H. R. M.; Nemati, Z. A. *J. Alloys Compd.* **2007**, *430*, 339−343.

(14) Krsmanovic, R.; Morozov, V. A.; Lebedev, O. I.; Polizzi, S.; Speghini, A.; Bettinelli, M.; Tendeloo, G. V. *Nanotechnology* **2007**, *18*, 325604/1−9.

(15) Mathur, S.; Shen, H.; Leleckaite, A.; Beganskiene, A.; Kareiva, A. *Mater. Res. Bull.* **2005**, *40*, 439−446.

(16) Chen, D.; Yu, Y.; Wang, Y.; Huang, P.; Weng, F. *J. Phys. Chem. C* **2009**, *113*, 6406−6410.

(17) Zhang, Q. Y.; Yang, C. H.; Pan, Y. X. *Appl. Phys. Lett.* **2007**, *90*, 021107/1−3.

(18) Liu, X.; Ye, S.; Qiao, Y.; Dong, G.; Zhu, B.; Chen, D.; Lakshminarayana, G.; Qiu, J. *Appl. Phys. B: Laser Opt.* **2009**, *96*, 51−55.

(19) Veith, M.; Mathur, S.; Kareiva, A.; Jilavi, M.; Zimmer, M.; Huch, V. *J. Mater. Chem.* **1999**, *9*, 3069−3079.

(20) Zhou, J.; Zhang, W.; Li, J.; Jiang, B.; Liu, W.; Pan, Y. *Ceram. Int.* **2010**, *36*, 193−197.

(21) Zhou, J.; Zhang, W.; Huang, T.; Wang, L.; Lia, J.; Liu, W.; Jiang, B.; Pan, Y.; Guo, J. *Ceram. Int.* **2011**, *37*, 513−519.

(22) Ueda, J.; Tanabe, S. *J. Appl. Phys.* **2009**, *106*, 043101/1−5.

(23) Zhou, J.; Teng, Y.; Liu, X.; Ye, S.; Maa, Z.; Qiu, J. *Phys. Chem. Chem. Phys.* **2010**, *12*, 13759−13762.

(24) Zhang, Q. Y.; Liang, X. F. *J. Soc. Inf. Disp.* **2008**, *16*, 755−758.

(25) Shao, L. M.; Jing, X. P. *ECS J. Solid State Sci. Technol.* **2012**, *1*, R22−R26.

(26) Song, P.; Jiang, C. *IEEE J. Quantum Electron.* **2013**, *49*, 634−640.

(27) Huang, X.; Han, S.; Huang, W.; Liu, X. *Chem. Soc. Rev.* **2013**, *42*, 173−201.

(28) Mishra, K.; Giri, N. K.; Rai, S. B. *Appl. Phys. B: Laser Opt.* **2011**, *103*, 863−875.

(29) Yao, G.; Su, L.; Xu, J.; Xu, X.; Zheng, L.; Cheng, Y. *J. Cryst. Growth* **2008**, *310*, 404−409.

(30) Cheng, B. M.; Yu, L.; Duan, C. K.; Wang, H.; Tanner, P. A. *J. Phys.: Cond. Mater.* **2008**, *20*, 345231/1−4.

(31) Hofmeister, A. M.; Campbell, K. R. *J. Appl. Phys.* **1992**, *72*, 638−646.

(32) Ekambaram, S.; Patil, K. C.; Maaza, M. *J. Alloys Compd.* **2005**, *393*, 81−92.

(33) Ye, S.; Zhou, J.; Wang, S.; Hu, R.; Wang, D.; Qiu, J. *Opt. Exp.* **2013**, *21*, 4167−4173.

(34) Lai, H.; Bao, A.; Yang, Y.; Tao, Y.; Yang, H.; Zhang, Y.; Han, L. *J. Phys. Chem. C* **2008**, *112*, 282−286.

(35) Pollnau, M.; Gamelin, D. R.; Luthi, S. R.; Gudel, H. U.; Hehlen, M. P. *Phys. Rev. B* **2000**, *61*, 3337−3346.

(36) Suyver, J. F.; Aebischer, A.; Garcia-Revilla, S.; Gerner, P.; Gudel, H. U. *Phys. Rev. B* **2005**, *71*, 125123/1−9.

(37) Liang, H.; Chen, G.; Li, L.; Liu, Y.; Qin, F.; Zhang, Z. *Opt. Commun.* **2009**, *282*, 3028−3031.

(38) Hoshina, T. *J. Chem. Phys.* **1969**, *50*, 5158−5162.

(39) Martın-Rodríguez, R.; Valiente, R.; Polizzi, S.; Bettinelli, M.; Speghini, A.; Piccinell, F. *J. Phys. Chem. C* **2009**, *113*, 12195−12200.

(40) Zhang, Q. Y.; Huang, X. Y. *Prog. Mater. Sci.* **2010**, *55*, 353−427.

(41) Strek, W.; Bednarkiewicz, A.; Deren, P. J. *J. Lumin.* **2001**, *92*, 229−235.
(42) Cheng, X.; Su, L.; Wang, Y.; Zhu, X.; Wei, X.; Wang, Y. *Opt. Mater.* **2012**, *34*, 1102−1106.